# A Direct Imaging Method for Electromagnetic Scattering Data without Phase Information *

Zhiming Chen† and Guanghui Huang‡

**Abstract.** In this paper we propose a direct imaging method based on reverse time migration for reconstructing extended obstacles by phaseless electromagnetic scattering data. We prove that the imaging resolution of the method is essentially the same as the imaging results using the scattering data with the full phase information. This implies the imaginary part of the cross-correlation imaging functional always peaks on the boundary of the obstacle. Numerical experiments are included to illustrate the powerful imaging quality.

**Key words.** Phaseless imaging, reverse time migration, electromagnetic wave

**AMS subject classifications.**

**1. Introduction.** Inverse scattering problems have wide applications in the community of radar imaging, biomedical tissue imaging, and nondestructive testings. Let the perfect conducting obstacle occupy a bounded Lipschitz domain $D \subset \mathbb{R}^3$ with $\nu$ the unit outer normal to its boundary $\Gamma_D$. Let $E^i$ be the incident wave and the total field $E = E^s + E^i$, where $E^s$ is the solution of the following electromagnetic scattering problem

$$\operatorname{curl}\operatorname{curl} E^s - k^2 E^s = 0 \quad \text{in } \mathbb{R}^3\backslash\bar{D}, \tag{1.1}$$

$$\nu \times E^s = -\nu \times E^i \quad \text{on } \Gamma_D, \tag{1.2}$$

$$r\,(\operatorname{curl} E^s \times \hat{x} - \mathbf{i}kE^s) \to 0 \quad \text{as } r = |x| \to \infty, \tag{1.3}$$

where $k > 0$ is the wave number and $\hat{x} = x/|x|$. The condition (1.3) is the outgoing Silver-Müller radiation condition which ensures the uniqueness of the physical solution. The existence and uniqueness of the solution $E^s \in H_{\rm loc}(\operatorname{curl}; \mathbb{R}^3\backslash\bar{D})$ of the problem (1.1)-(1.3) is a well studied subject in the literature [13, 23]. We remark that the results in this paper also apply to penetrable obstacles or non-penetrable obstacles with other boundary conditions on the scatterer.

In the diffractive optics imaging and radar imaging system, it is easier to measure the accurate intensity of the scattering field than the phase information of the field [2, 15, 22, 18, 14, 31]. Thus it is very desirable to develop efficient numerical methods for reconstructing the obstacle with only phaseless data. In this paper, we consider reconstructing the shape of the extended obstacle with only the amplitude information of the total field, i.e. phaseless data $|E|$. There exist several iterative methods for reconstruction of the obstacles with phaseless data, cf. e.g. [21, 19]. However, because of the non-convexity of the misfit functional, local

*This work is supported by National Basic Research Project under the grant 2011CB309700 and China NSF under the grants 11021101 and 11321061.

†LSEC, Institute of Computational Mathematics and Scientific Engineering Computing, Academy of Mathematics and System Sciences, Chinese Academy of Sciences, Beijing 100190, P.R. CHINA (zmchen@lsec.cc.ac.cn).

‡The Rice Inversion Project, Department of Computational and Applied Mathematics, Rice University, Houston, TX 77005-1892, USA (ghhuang@rice.edu).

**Figure 1.** *Schematic for the phaseless electromagnetic field data acquisition.*

minima may arise and lead to a wrong solution to the inverse problem. Under the condition that the scattered field is small compared to the incident field, [1] proposes a phaseless imaging method by first recovering the phase information of the scattered field by solving a simple least square problem and then using Kirchhoff migration for imaging. For imaging localized small scatterers using only intensity measurements, [7] formulates the imaging problem as a non-convex optimization problem that has an exact recovery and [25] proposes an approach by first restoring the full time reversal matrix and then using the conventional MUSIC algorithm to find the localized scatterers. The non-convex optimization problem in [7] is further replaced by a convex optimization problem. We also refer to the phase retrieval method in [16, 6] and the references therein for finding the missing phase information from the knowledge of the modulus of both the function and its Fourier transform.

The reverse time migration (RTM) method, which consists of back-propagating the complex conjugated scattering field into the background medium and computing the cross-correlation between the incident wave field and the backpropagated field to output the final imaging profile, is nowadays a standard imaging technique widely used in seismic imaging [3]. In [9, 10, 11], the RTM method for reconstructing extended targets using acoustic, electromagnetic and elastic waves at a fixed frequency is proposed and studied. The resolution analysis in [9, 10, 11] is achieved without the small inclusion or geometrical optics assumption previously made in the literature.

Let $\Gamma_s = \partial B_s$ and $\Gamma_r = \partial B_r$, where $B_s, B_r$ are the balls centered at the origin of radius $R_s, R_r$, respectively. We denote by $\Omega$ the sampling domain in which the obstacle is sought, see Figure 1 for the geometric illustration of the problem. Without loss of generality we assume $R_r = \tau R_s, \tau \geq 1$. We remark that the case $\tau \leq 1$ can be considered by the same method in

this paper. The imaging function for the electromagnetic waves studied in [10] is

$$I_{\rm RTM}(z) = -k^2 {\rm Im} \int_{\Gamma_r} \int_{\Gamma_s} g(z,x_s) p \cdot \mathbb{G}(z,x_r)^T \overline{E^s(x_r,x_s)} ds(x_s) ds(x_r), \tag{1.4}$$

where $g(x,y) = \frac{e^{{\rm i}k|x-y|}}{4\pi|x-y|}$ is the fundamental solution of the 3D Helmholtz equation and $\mathbb{G}(x,y)$ is the dyadic Green function for the time harmonic Maxwell equation (see (2.2) below). $E^s(x,x_s)$ is the solution of (1.1)-(1.3) with the incident wave $E^i(x,x_s) = \mathbb{G}(x,x_s)p$, where $p$ is a unit polarization vector. It is shown in [10] that $I_{\rm RTM}(z)$ always peaks on the boundary of the scatterer and decays when $z$ moves away from the scatterer.

In [12], the authors proposed a reliable imaging method based on reverse time migration for acoustic waves using only phaseless total field data and obtained quite impressive imaging results. In this paper we extend the idea in [12] to electromagnetic waves and propose the following imaging function for phaseless imaging using electromagnetic waves

$$I^{\rm phaseless}_{\rm RTM}(z) = -k^2 \, {\rm Im} \int_{\Gamma_s} \int_{\Gamma_r} g(z,x_s) g(x_r,z) D_\varepsilon(x_r,x_s) ds(x_r) ds(x_s), \quad \forall \ z \in \Omega, \tag{1.5}$$

where $\varepsilon = (kR_s)^{-1}$ and $D_\varepsilon(x_r,x_s)$ is the corrected data depending only on the phaseless total field data $|E(x_r,x_s)\cdot p|$ (see (2.5) below). We will show that $I^{\rm phaseless}_{\rm RTM}(z) = I_{\rm RTM}(z) + O(|\ln(kR_s)|^2 R_s^{-1})$ in Theorem 4.1 which implies the imaging output of our new algorithm is essentially the same as the imaging results using the scattering data with the full phase information when $R_s \gg 1$. To the best of the authors knowledge, this is the first attempt in the literature to develop a direct imaging method for reconstructing extended obstacles by using phaseless electromagnetic scattering data only.

The rest of this paper is organized as follows. In section 2 we introduce our RTM algorithm for imaging the obstacle with phaseless electromagnetic total field data. In section 3 we introduce some preliminary results on the forward problem and the imaging function $I_{\rm RTM}(z)$. In section 4 we consider the resolution of our algorithm for imaging perfectly conducting obstacles. In section 5 we report several numerical experiments to show the imaging results of our phaseless electromagnetic RTM algorithm in 2D and 3D. In the appendix we consider the high frequency limit of the RTM imaging function.

**2. Reverse time migration method.** In this section we introduce the RTM method for inverse scattering problems with phaseless electromagnetic scattering data. We assume that there are $N_s$ emitters and $N_r$ transducers uniformly distributed on $\Gamma_s$ and $\Gamma_r$, respectively. We assume the obstacle $D$ is contained in the search domain $\Omega$ and $\Omega$ is inside $B_s, B_r$. Without loss of generality we assume $R_r = \tau R_s, \tau \geq 1$.

Let $\mathbb{G}(x,y) \in \mathbb{C}^{3\times 3}$ be the dyadic Green function to the time harmonic Maxwell equation

$$\mathbb{G}(x,y) = g(x,y)\mathbb{I} + \frac{\nabla_x \nabla_x}{k^2} g(x,y), \tag{2.1}$$

where $\mathbb{I}$ is the $\mathbb{R}^{3\times 3}$ identity matrix and $g(x,y) = \frac{e^{{\rm i}k|x-y|}}{4\pi|x-y|}$ is the fundamental solution of 3D Helmholtz equation. Direct calculation shows that

$$\mathbb{G}(x,y) = (\mathbb{I} - J(x,y)J(x,y)^T) g(x,y) + \mathbb{A}(x,y) g(x,y), \tag{2.2}$$

where $J(x,y)=\frac{x-y}{|x-y|}$ and $\mathbb{A}(x,y)=(\frac{\mathbf{i}}{k|x-y|}-\frac{1}{k^2|x-y|^2})(\mathbb{I}-3J(x,y)J(x,y)^T)$.

Let the incident wave $E^i(x,x_s)=\mathbb{G}(x,x_s)p$ with the unit polarization vector $p$. The measurement $|E(x_r,x_s)\cdot p|$ is the modulus of the total field $E(x_r,x_s)=E^s(x_r,x_s)+E^i(x_r,x_s)$ in the polarization $p$, where $E^s(x,x_s)$ is the solution of the Maxwell scattering problem (1.1)-(1.3) with the incident wave $E^i(x)=E^i(x,x_s)$. We additionally assume that $x_s\neq x_r$ to avoid the singularity of the incident point source field $E^i(x,x_s)$ measured at $x_r$, which can be easily satisfied in practical applications.

For any $\varepsilon>0$, denote

$$\Theta_\varepsilon:=\left\{(\hat{x}_r,\hat{x}_s)\in S^2\times S^2:|\tau\hat{x}_r-\hat{x}_s|>\varepsilon \text{ and } 1-|J(\tau\hat{x}_r,\hat{x}_s)\cdot p|^2>\varepsilon\right\}, \tag{2.3}$$

where $S^2$ is the unit sphere in $\mathbb{R}^3$. Obviously, $J(x_r,x_s)=J(\tau\hat{x}_r,\hat{x}_s)$ for $(x_r,x_s)\in\Gamma_r\times\Gamma_s$. We define, for $(x_r,x_s)\in\Gamma_r\times\Gamma_s$,

$$\beta_\varepsilon(x_r,x_s)=\begin{cases}(1-|J(x_r,x_s)\cdot p|^2)^{-1} & \text{if } (\hat{x}_r,\hat{x}_s)\in\Theta_\varepsilon,\\ 0 & \text{otherwise.}\end{cases} \tag{2.4}$$

(2.3)-(2.4) serve to select certain sources and receivers for our phaseless RTM functional. The first condition in the set $\Theta_\varepsilon$ is to avoid the singularity of the data and the second condition is introduced to cancel the amplitude effect of the incident electromagnetic wave (see the Green function in (2.2)). The importance of the selection will be clear for dealing with the second and third terms in (4.2) by using (4.3) below.

Our imaging algorithm consists of back-propagating the corrected data

$$D_\varepsilon(x_r,x_s)=(|E(x_r,x_s)\cdot p|^2-|E^i(x_r,x_s)\cdot p|^2)\frac{\beta_\varepsilon(x_r,x_s)}{g(x_r,x_s)} \tag{2.5}$$

into the domain using the fundamental solution $g(x_r,z)$ and computing the imaginary part of the cross-correlation between $g(z,x_s)$ and the back-propagated field.

Algorithm 2.1.(RTM FOR PHASELESS ELECTROMAGNETIC SCATTERING DATA)
*Given the data $|E(x_r,x_s)\cdot p|$ which is the modulus of the total field $E(x,x_s)$ in the unit polarization $p$ at $x_r$ with the point source excitation $E^i(x,x_s)=\mathbb{G}(x,x_s)p$, $s=1,\dots,N_s$, $r=1,\dots,N_r$. Set $\varepsilon=(kR_s)^{-1}$.*
1° *Back-propagation: For $s=1,\dots,N_s$, compute the back-propagation field*

$$F_b(z,x_s)=-\frac{1}{N_r}\sum_{r=1}^{N_r}|\Delta(x_r)|\ g(x_r,z)D_\varepsilon(x_r,x_s),\qquad\forall\ z\in\Omega, \tag{2.6}$$

*where $|\Delta(x_r)|=2\pi^2R_r^2\sin\theta_r$ is the surface element at $x_r$.*
2° *Cross-correlation: For $z\in\Omega$, compute*

$$I(z)=k^2\,\mathrm{Im}\left\{\frac{1}{N_s}\sum_{s=1}^{N_s}|\Delta(x_s)|\ g(z,x_s)F_b(z,x_s)\right\}, \tag{2.7}$$

*where $|\Delta(x_s)|=2\pi^2R_s^2\sin\theta_s$ is the surface element at $x_s$.*

The dimensionless parameter $\varepsilon$ chosen here is based on our error estimate in Theorem 4.1, which states our new method with phaseless data is asymptotically identical to the RTM method with full phase information with the error of order $|\ln(kR_s)|^2 R_s^{-1}$ if one chooses $\varepsilon = (kR_s)^{-1}$.

We remark that $F_b(\cdot, x_s)$ is the scattering solution of the following Helmholtz equation

$$\Delta F_b(x, x_s) - k^2 F_b(x, x_s) = \frac{1}{N_r} \sum_{r=1}^{N_r} |\Delta(x_r)| D_\varepsilon(x_r, x_s) \delta_{x_r}(x).$$

It is easy to see that

$$I(z) = -k^2 \operatorname{Im} \left\{ \frac{1}{N_s N_r} \sum_{s=1}^{N_s} \sum_{r=1}^{N_r} |\Delta(x_r)| \, |\Delta(x_s)| \, g(z, x_s) g(x_r, z) D_\varepsilon(x_r, x_s) \right\}. \tag{2.8}$$

This is the formula used in our numerical experiments in section 5. By letting $N_s, N_r \to \infty$, we know that (2.8) can be viewed as an approximation to the continuous integral defined in (1.5).

To conclude this section, we show some preliminary properties of the function $\beta_\varepsilon(x_r, x_s)$.

Lemma 2.1. *There exists a constant $C$ independent of $k$ and $\tau$ such that $|(S^2 \times S^2) \backslash \bar{\Theta}_\varepsilon| \leq C\varepsilon$, and*

$$\left| \int_{S^2 \times S^2} \beta_\varepsilon(x_r, x_s) d\hat{x}_r d\hat{x}_s \right| \leq C |\ln \varepsilon|, \tag{2.9}$$

$$\left| \int_{S^2 \times S^2} |\mathbb{A}(x_r, x_s) p \cdot p| \beta_\varepsilon(x_r, x_s) d\hat{x}_r d\hat{x}_s \right| \leq C (kR_s)^{-1} |\ln \varepsilon|^2. \tag{2.10}$$

*Proof.* We use a coordinate transform for double integral over spheres introduced in [5]. Let $r = |\tau \hat{x}_r - \hat{x}_s|$ and $\hat{y} \in S^2$ such that $\tau \hat{x}_r - \hat{x}_s = r\hat{y}$ and $\psi$ be the unit vector lying in the plane spanned by $\hat{x}_r, \hat{x}_s, \hat{y}$ and is perpendicular to $\hat{y}$. By [5, (2.8)]

$$d\hat{x}_r d\hat{x}_s = \frac{1}{\tau} r dr d\psi d\hat{y}, \quad r \in (\tau - 1, \tau + 1), \psi \in S^1, \hat{y} \in S^2. \tag{2.11}$$

By (2.3) we know that $\Theta_\varepsilon = \{(\hat{x}_r, \hat{x}_s) \in S^2 \times S^2 : r > \varepsilon \text{ and } 1 - |\hat{y} \cdot p|^2 > \varepsilon\}$. Then

$$|(S^2 \times S^2) \backslash \bar{\Theta}_\varepsilon| \leq \frac{1}{\tau} \int_{r<\varepsilon} \int_{S^1} \int_{S^2} r dr d\psi d\hat{y} + \frac{1}{\tau} \int_{\tau-1}^{\tau+1} \int_{S^1} \int_{1-|\hat{y}\cdot p|^2<\varepsilon} r dr d\psi d\hat{y}.$$

The first term is obviously bounded by $C\varepsilon^2$. To estimate the second integral, let $\mathbb{Q} \in \mathbb{R}^{3\times 3}$ be the orthogonal matrix such that $\mathbb{Q}p = (0, 0, 1)^T$. We denote the spherical coordinates of $\mathbb{Q}\hat{y} = (\sin\theta\cos\phi, \sin\theta\sin\phi, \cos\theta)^T$, $\theta \in [0, \pi], \phi \in [0, 2\pi]$. Clearly $1 - |\hat{y} \cdot p|^2 = \sin^2\theta$. This implies

$$\frac{1}{\tau} \int_{\tau-1}^{\tau+1} \int_{S^1} \int_{1-|\hat{y}\cdot p|^2<\varepsilon} r dr d\psi d\hat{y} \leq C \int_0^{2\pi} \int_{\sin^2\theta<\varepsilon} \sin\theta d\theta d\phi \leq C\varepsilon.$$

This shows $|(S^2 \times S^2)\backslash\bar{\Theta}_\varepsilon| \le C\varepsilon$.

Now we show (2.9). Since $\beta_\varepsilon(x_r, x_s) = (1 - |\hat{y} \cdot p|^2)^{-1}\chi_{\Theta_\varepsilon}$, where $\chi_{\Theta_\varepsilon}$ is the characteristic function of $\Theta_\varepsilon$, we know that

$$\begin{aligned}\int_{S^2\times S^2} \beta_\varepsilon(x_r, x_s) d\hat{x}_r d\hat{x}_s &\le \frac{1}{\tau}\int_{\tau-1}^{\tau+1}\int_{S^1}\int_{1-|\hat{y}\cdot p|^2>\varepsilon}(1 - |\hat{y}\cdot p|^2)^{-1} r dr d\psi d\hat{y}\\ &\le C\int_{1-|\hat{y}\cdot p|^2>\varepsilon}(1 - |\hat{y}\cdot p|^2)^{-1} d\hat{y},\\ &= C\int_0^{2\pi}\int_{\sin^2\theta>\varepsilon}\frac{1}{\sin\theta} d\theta d\phi.\end{aligned}$$

This yields (2.9). The estimate (2.10) can be proved similarly by the definition of $\mathbb{A}(x_r, x_s)$ in (2.2). We omit the details. ■

**3. Preliminary results.** In this section introduce some preliminary results on the forward scattering problem (1.1)-(1.3) and the imaging function $I_{\mathrm{RTM}}(z)$ in (1.4). We start by introducing some notation. Let $\mathcal{D} \subset \mathbb{R}^3$ be a Lipschitz domain with boundary $\Gamma$ whose unit outer normal is denoted by $n$. The space $H(\mathrm{curl};\mathcal{D}) = \{u \in L^2(\mathcal{D})^3 : \mathrm{curl}\, u \in L^2(\mathcal{D})^3\}$ is a Hilbert space under the norm $\|u\|_{H(\mathrm{curl};\mathcal{D})} = (\|u\|^2_{L^2(\mathcal{D})} + \|\mathrm{curl}\, u\|^2_{L^2(\mathcal{D})})^{1/2}$. For any $u \in H(\mathrm{curl};\mathcal{D})$, the tangential trace $\gamma_\tau u = n \times u|_\Gamma$ is a surjective mapping to the space

$$H^{-1/2}(\mathrm{div};\Gamma) = \{\lambda \in V_\pi(\Gamma)' : \mathrm{div}_\Gamma \lambda \in H^{-1/2}(\Gamma)\},$$

which is a Hilbert space under the norm $\|\lambda\|_{H^{-1/2}(\mathrm{div};\Gamma)} = (\|\lambda\|^2_{V_\pi(\Gamma)'} + \|\mathrm{div}_\Gamma\lambda\|^2_{H^{-1/2}(\Gamma)})^{1/2}$ (see e.g. [4]) . Here $V_\pi(\Gamma)'$ is the dual space of $V_\pi(\Gamma) = \pi(H^{1/2}(\Gamma)^3)$, where for any $u \in H^{1/2}(\Gamma)^3$, $\pi(u) = n \times u \times n$. In the following, we will use the weighted $H^{1/2}(\Gamma)$ norm

$$\| v \|_{H^{1/2}(\Gamma)} = \left( d_{\mathcal{D}}^{-1} \| v \|^2_{L^2(\Gamma)} + \int_\Gamma\int_\Gamma \frac{|v(x) - v(x')|^2}{|x - x'|^3}\, ds(x) ds(x') \right)^{1/2},$$

and the weighted $H^{-1/2}(\mathrm{div};\Gamma)$ norm

$$\| \mu \|_{H^{-1/2}(\mathrm{div};\Gamma)} = \left( d_{\mathcal{D}}^{-2}\|\mu\|^2_{V_\pi'(\Gamma)} + \|\mathrm{div}_\Gamma\mu\|^2_{H^{-1/2}(\Gamma)} \right)^{1/2},$$

where $d_{\mathcal{D}}$ is the diameter of $\mathcal{D}$. By the scaling argument and the trace theorem we know that there exists constant $C > 0$ independent of $d_{\mathcal{D}}$, such that

$$\|\phi\|_{H^{1/2}(\Gamma_{\mathcal{D}})} \le C d_{\mathcal{D}}^{1/2} \max_{x\in\bar{\mathcal{D}}}(|\phi(x)| + d_{\mathcal{D}}|\nabla\phi(x)|), \quad \forall \phi \in C^1(\bar{\mathcal{D}}), \tag{3.1}$$

$$\| \nu \times u \|_{H^{-1/2}(\mathrm{div};\Gamma_{\mathcal{D}})} \le C d_{\mathcal{D}}^{1/2} \max_{x\in\bar{\mathcal{D}}}(|u(x)| + d_{\mathcal{D}}|\mathrm{curl}\, u(x)|), \quad \forall u \in C^1(\bar{\mathcal{D}})^3. \tag{3.2}$$

Now we recall the definition of the Dirichlet-to-Neumann mapping for Maxwell scattering problems [23]. For any $g \in H^{-1/2}(\mathrm{div};\Gamma_D)$, define $G_e(g) = \frac{1}{\mathbf{i}k}\nu \times \mathrm{curl}\, U$ on $\Gamma_D$, where $U \in H_{\mathrm{loc}}(\mathrm{curl}\,;\mathbb{R}^3\backslash\bar{D})$ is the solution of the problem:

$$\mathrm{curl}\,\mathrm{curl}\, U - k^2 U = 0 \quad \text{in } \mathbb{R}^3\backslash\bar{D}, \tag{3.3}$$

$$\nu \times U = g \ \text{ on } \Gamma_D, \quad r\,(\mathrm{curl}\, U \times \hat{x} - \mathbf{i}kU) \to 0 \quad \text{as } r \to \infty. \tag{3.4}$$

It is known that $G_e : H^{-1/2}(\mathrm{div};\Gamma_D) \to H^{-1/2}(\mathrm{div};\Gamma_D)$ is a bounded linear operator for which we will denote $\|G_e\|$ by its operator norm in the remainder of this paper.

The far field pattern $U^\infty(\hat{x})$ of the solution $U$ to the scattering problem (3.3)-(3.4) is defined as [13, Theorem 6.8]

$$U^\infty(\hat{x}) = \frac{1}{4\pi}\hat{x} \times \int_{\Gamma_D} \Big[\nu(y) \times \mathrm{curl}\, U(y) \times \hat{x} + \mathbf{i}k\nu(y) \times U(y)\Big] e^{-\mathbf{i}k\hat{x}\cdot y} ds(y). \tag{3.5}$$

In the following, we will always use the superscript $\infty$ to denote the far field pattern of scattering solutions. The following lemma is essentially proved in [13, Theorem 6.8]. We will give a sketch of the proof in the appendix of this paper.

Lemma 3.1. *Let $U$ be the solution of (3.3)-(3.4). Then the following asymptotic behavior is valid*

$$U(x) = \frac{e^{\mathbf{i}k|x|}}{|x|} U^\infty(\hat{x}) + \gamma(x), \qquad \forall x \in \mathbb{R}^3\backslash\bar{D},\ |x| \gg 1, \tag{3.6}$$

*where $|\gamma(x)| \le C d_D^{3/2}(1 + \|G_e\|)|x|^{-2}\|g\|_{H^{-1/2}(\mathrm{div};\Gamma_D)}$ for some constant $C$ depending on $kd_D$ but independent of $k, d_D$.*

The following identity for the solution of (3.3)-(3.4) is well-known, see e.g. [10, Lemma 3.4].

$$\mathrm{Im}\,\langle \nu \times U \times \nu, \nu \times \mathrm{curl}\, U\rangle_{\Gamma_D} = k \int_{S^2} |U^\infty(\hat{x})|^2 d\hat{x}, \tag{3.7}$$

where $\langle\cdot,\cdot\rangle_{\Gamma_D}$ is the duality pairing between $H^{-1/2}(\mathrm{curl}\,;\Gamma_D)$ and $H^{-1/2}(\mathrm{div};\Gamma_D)$.

The following corollary of the Helmholtz-Kirchhoff identity in [10, Lemma 3.2] plays a key role in the analysis of the imaging resolution of the RTM method for imaging extended targets using electromagnetic waves with full phase information.

Lemma 3.2. *We have*

$$k \int_{\Gamma_s} \overline{g(z,x_s)}\mathbb{G}(x,x_s)\, ds(x_s) = \mathrm{Im}\,\mathbb{G}(x,z) + \mathbb{W}_s(x,z), \qquad \forall x,z \in \Omega,$$

*where $|w_s^{ij}(x,z)| + k^{-1}|\nabla_x w_s^{ij}(x,z)| \le C R_s^{-1}$ for some constant $C$ depending on $k|x|, k|z|$ but independent of $k$. Here $w_s^{ij}(x,z)$ is the $(i,j)$-element of the matrix $\mathbb{W}_s(x,z)$, $i,j = 1,2,3$.*

For the sake of convenience, we introduce the following notation:

$$\mathcal{G}(W,U) = \int_{\Gamma_D} [W(x)\cdot\nu \times \mathrm{curl}\, U(x) - \nu \times \mathrm{curl}\, W(x)\cdot U(x)]\, ds(x). \tag{3.8}$$

Using this notation, the integral representation formula of the solution $U(x)$ to the scattering problem (3.3)-(3.4) reads: $U(x)\cdot q = \mathcal{G}(\mathbb{G}(x,\cdot)q, U)$, for any $x \in \mathbb{R}^3\backslash\bar{D}, q \in S^2$.

Lemma 3.3. *Let $W \in C^1(\bar{D})^3$ and $U \in H_{\mathrm{loc}}(\mathrm{curl};\mathbb{R}^3\backslash\bar{D})$ be the solution of the scattering problem (3.3)-(3.4) with the boundary condition $g = \nu \times u$ on $\Gamma_D$ for some function $u \in C^1(\bar{D})^3$. Then we have*

$$|\mathcal{G}(W,U)| \le C d_D(1 + \|G_e\|) \max_{x\in\bar{D}} [(|W(x)| + d_D|\nabla W(x)|)(|u(x)| + d_D|\mathrm{curl}\, u(x)|)]$$

*for some constant $C$ depending on $kd_D$ but independent of $k, d_D$.*

*Proof.* By (3.2) and the definition of the Dirichlet-to-Neumann mapping we have

$$\begin{aligned}
&\left|\int_{\Gamma_D} W(x)\cdot \nu\times \operatorname{curl} U(x) ds(x)\right| \\
&\le d_D\|W\|_{V_\pi(\Gamma_D)}\|\nu\times \operatorname{curl} U\|_{H^{-1/2}(\operatorname{div};\Gamma_D)} \\
&\le Ckd_D\|G_e\|\|W\|_{H^{1/2}(\Gamma_D)}\|\nu\times u\|_{H^{-1/2}(\operatorname{div};\Gamma_D)} \\
&\le Cd_D\|G_e\|\max_{x\in\bar D}[(|W(x)|+d_D|\nabla W(x)|)(|u(x)|+d_D|\operatorname{curl} u(x)|)].
\end{aligned}$$

On the other hand,

$$\left|\int_{\Gamma_D} \nu\times \operatorname{curl} W(x)\cdot U(x) ds(x)\right| \le Cd_D^2\max_{x\in\Gamma_D}(|\operatorname{curl} W(x)|\cdot|u(x)|).$$

This completes the proof. ■

The following theorem for the imaging function $I_{\rm RTM}(z)$ in (1.4) can be proved by the method in [10] where the analysis for penetrable and impedance non-penetrable obstacles is given. The extension to the case of perfect conducting obstacles considered in (1.1)-(1.3) is similar and is omitted here.

Theorem 3.1. *For any $z\in\Omega$, let $\Psi(x,z)$ be the scattering solution to the problem*

$$\operatorname{curl}\operatorname{curl}\Psi(x,z)-k^2\Psi(x,z)=0 \quad \text{in } \mathbb{R}^3\backslash\bar D, \tag{3.9}$$

$$\nu\times\Psi(x,z)=-\nu\times[\operatorname{Im}\mathbb{G}(x,z)p] \quad \text{on } \Gamma_D, \tag{3.10}$$

$$r\Big(\operatorname{curl}\Psi(x,z)\times\hat x-\mathbf{i}k\Psi(x,z)\Big)\to 0, \qquad \text{as } \ r\to+\infty. \tag{3.11}$$

*Then we have*

$$I_{\rm RTM}(z)=k\int_{S^2}|\Psi^\infty(\hat x,z)|^2d\hat x+R_{\rm RTM}(z), \qquad \forall z\in\Omega,$$

*where $\|R_{\rm RTM}\|_{L^\infty(\Omega)}\le C(1+\|G_e\|)R_s^{-1}$ for some constant $C$ that may depend on $kd_D, k|z|$ but is independent of $k, R_r, R_s$.*

We remark that $\Psi(x,z)$ is the scattering solution of the problem (3.9)-(3.11) with the incoming wave $\operatorname{Im}\mathbb{G}(x,z)p$. Since $\operatorname{Im}\mathbb{G}(x,z)p=\left[(\mathbb{I}+\frac{\nabla_x\nabla_x}{k^2})\frac{\sin(k|x-z|)}{4\pi|x-z|}\right]p$ which peaks when $x=z$ and decays as $|x-z|$ becomes large, the source of (3.9)-(3.11) becomes small when $z$ moves away from $\partial D$ outside the scatterer. Therefore the imaging function $I_{\rm RTM}(z)$ will have a contrast at the boundary of the scatterer $D$ and decay away from the scatterer which is confirmed by the numerical results in [10]. The high frequency analysis for the imaging function in the appendix of this paper reveals that for $z\in\Gamma_D$, $I_{\rm RTM}(z)$ is inversely proportional to the Gauss curvature of the boundary around $z$ (see (6.2) in the appendix).

From Theorem 3.1 we know that the RTM imaging functional $I_{\rm RTM}(z)$ is asymptotically proportional to the integration of the far field pattern over all directions when the incoming wave is $\operatorname{Im}\mathbb{G}(\cdot,z)p$. This incoming wave is the point spread function (PSF) for imaging a point source $z$ by incident waves $\mathbb{G}(x,\cdot)p$ (see Lemma 3.2 which is the consequence of the Helmholtz-Kirchhoff identity). As PSF describes the resolution of the imaging of a point source, we call the conclusion of Theorem 3.1 the resolution analysis as it essentially describes the sharpness of the image for imaging extended obstacles by the RTM algorithm.

**4. Resolution analysis for the phaseless RTM algorithm.** In this section we prove the following theorem which shows that our RTM algorithm for phaseless electromagnetic scattering data is the same as the RTM algorithm using scattering data with full phase information.

Theorem 4.1. *Let $\varepsilon = (kR_s)^{-1}$. For any $z \in \Omega$, we have*

$$|I_{\rm RTM}^{\rm phaseless}(z) - I_{\rm RTM}(z)| \le C(1 + \|G_e\|)^2 |\ln(kR_s)|^2 R_s^{-1} \tag{4.1}$$

*for some constant $C$ that may depend on $kd_D, k|z|$ but is independent of $k, R_r, R_s$.*

The proof of this theorem depends on several lemmas that follow. We first observe that

$$\begin{aligned} D_\varepsilon(x_r, x_s) &= (|E(x_r, x_s) \cdot p|^2 - |E^i(x_r, x_s) \cdot p|^2) \frac{\beta_\varepsilon(x_r, x_s)}{g(x_r, x_s)} \\ &= \big(|E^s \cdot p|^2 + (E^s \cdot p)(\overline{E}^i \cdot p) + (\overline{E}^s \cdot p)(E^i \cdot p)\big)(x_r, x_s) \frac{\beta_\varepsilon(x_r, x_s)}{g(x_r, x_s)}. \end{aligned}$$

This yields

$$\begin{aligned} I_{\rm RTM}^{\rm phaseless}(z) \;=\; & -k^2 \,{\rm Im} \int_{\Gamma_r \times \Gamma_s} g(z, x_s) g(x_r, z) |E^s(x_r, x_s) \cdot p|^2 \frac{\beta_\varepsilon(x_r, x_s)}{g(x_r, x_s)} \\ & -k^2 \,{\rm Im} \int_{\Gamma_r \times \Gamma_s} g(z, x_s) g(x_r, z) (\overline{E^s(x_r, x_s)} \cdot p)(E^i(x_r, x_s) \cdot p) \frac{\beta_\varepsilon(x_r, x_s)}{g(x_r, x_s)} \\ & -k^2 \,{\rm Im} \int_{\Gamma_r \times \Gamma_s} g(z, x_s) g(x_r, z) (E^s(x_r, x_s) \cdot p)(\overline{E^i(x_r, x_s)} \cdot p) \frac{\beta_\varepsilon(x_r, x_s)}{g(x_r, x_s)} \\ :=\; & {\rm I} + {\rm II} + {\rm III}. \end{aligned} \tag{4.2}$$

Lemma 4.1. *We have $|E^s(x_r, x_s)| \le C d_D (1 + \|G_e\|)(R_r R_s)^{-1}$ uniformly for $x_r \in \Gamma_r, x_s \in \Gamma_s$, where the constant $C$ depends on $kd_D$ but is independent of $k$.*

*Proof.* By the integral representation formula, for any $q \in S^2$,

$$E^s(x_r, x_s) \cdot q = \mathcal{G}(\mathbb{G}(x_r, \cdot)q, E^s(\cdot, x_s)).$$

Since $\nu \times E^s(x, x_s) = -\nu \times (\mathbb{G}(x, x_s)p)$ on $\Gamma_D$, the lemma follows easily from Lemma 3.3. ■

By Lemma 4.1 and Lemma 2.1 one obtains the following estimate for the first term in (4.2).

Lemma 4.2. *Let $\varepsilon = (kR_s)^{-1}$. We have $|{\rm I}| \le C(1+\|G_e\|)^2 R_s^{-1} |\ln(kR_s)|$, where the constant $C$ depends on $kd_D$ but is independent of $k$.*

Now we consider the other two terms in (4.2). Since $\beta_\varepsilon(x_r, x_s) = (1 - |J(x_r, x_s) \cdot p|^2)^{-1} \chi_{\Theta_\varepsilon}$, by (2.2) we have

$$E^i(x_r, x_s) \cdot p \, \frac{\beta_\varepsilon(x_r, x_s)}{g(x_r, x_s)} = \chi_{\Theta_\varepsilon} + (\mathbb{A}(x_r, x_s)p \cdot p)\beta_\varepsilon(x_r, x_s). \tag{4.3}$$

This implies

$$\begin{aligned}\mathrm{II} =& -k^2\mathrm{Im}\int_{\Gamma_r\times\Gamma_s} g(z,x_s)g(x_r,z)\overline{E^s(x_r,x_s)}\cdot p ds(x_s)ds(x_r)\\ &-k^2\,\mathrm{Im}\int_{\Gamma_r\times\Gamma_s} g(z,x_s)g(x_r,z)\overline{E^s(x_r,x_s)}\cdot p(\chi_{\Theta_\varepsilon}-1)ds(x_r)ds(x_s)\\ &-k^2\,\mathrm{Im}\int_{\Gamma_r\times\Gamma_s} g(z,x_s)g(x_r,z)\overline{E^s(x_r,x_s)}\cdot p[(\mathbb{A}(x_r,x_s)p\cdot p)\beta_\varepsilon(x_r,x_s)]ds(x_r)ds(x_s)\\ :=&\ \mathrm{II}_1+\mathrm{II}_2+\mathrm{II}_3.\end{aligned}\tag{4.4}$$

Similarly,

$$\begin{aligned}\mathrm{III} =& -k^2\,\mathrm{Im}\int_{\Gamma_r\times\Gamma_s} g(z,x_s)g(x_r,z)E^s(x_r,x_s)\cdot p\frac{\overline{g(x_r,x_s)}}{g(x_r,x_s)}ds(x_r)ds(x_s)\\ &-k^2\,\mathrm{Im}\int_{\Gamma_r\times\Gamma_s} g(z,x_s)g(x_r,z)E^s(x_r,x_s)\cdot p(\chi_{\Theta_\varepsilon}-1)\frac{\overline{g(x_r,x_s)}}{g(x_r,x_s)}ds(x_r)ds(x_s)\\ &-k^2\,\mathrm{Im}\int_{\Gamma_r\times\Gamma_s} g(z,x_s)g(x_r,z)E^s(x_r,x_s)\cdot p(\overline{\mathbb{A}(x_r,x_s)}p\cdot p)\beta_\varepsilon(x_r,x_s)\frac{\overline{g(x_r,x_s)}}{g(x_r,x_s)}\\ :=&\ \mathrm{III}_1+\mathrm{III}_2+\mathrm{III}_3.\end{aligned}\tag{4.5}$$

Lemma 4.3. *Let $\varepsilon=(kR_s)^{-1}$. We have $|\mathrm{II}_2+\mathrm{III}_2|\le C(1+\|G_e\|)R_s^{-1}$, where the constant $C$ depends on $kd_D$ but is independent of $k$.*

*Proof.* By Lemma 4.1 and Lemma 2.1 we know that

$$\begin{aligned}|\mathrm{II}_2+\mathrm{III}_2|&\le Ck^2d_D(1+\|G_e\|)(R_rR_s)^{-2}\int_{\Gamma_r\times\Gamma_s}(\chi_{\Theta_\varepsilon}-1)ds(x_r)ds(x_s)\\ &= Ck(1+\|G_e\|)|(S^2\times S^2)\backslash\bar{\Theta}_\varepsilon|.\end{aligned}$$

This completes the proof by Lemma 4.3. ■

Lemma 4.4. *Let $\varepsilon=(kR_s)^{-1}$. We have $|\mathrm{II}_3+\mathrm{III}_3|\le C(1+\|G_e\|)R_s^{-1}|\ln(kR_s)|^2$, where the constant $C$ depends on $kd_D$ but is independent of $k$.*

*Proof.* By Lemma 4.1 and (2.10) in Lemma 2.1 we have

$$\begin{aligned}|\mathrm{II}_3+\mathrm{III}_3|&\le Ck^2d_D(1+\|G_e\|)(R_rR_s)^{-2}\int_{\Gamma_r\times\Gamma_s}|\mathbb{A}(x_r,x_s)p\cdot p|\beta_\varepsilon(x_r,x_s)ds(x_r)ds(x_s)\\ &\le C(1+\|G_e\|)R_s^{-1}|\ln\varepsilon|^2.\end{aligned}$$

This completes the proof. ■

Now we proceed to estimate the term $\mathrm{III}_1$. We need the following mixed reciprocity relation of electromagnetic waves. Let $E^i_{\mathrm{pl}}(x,d_s,q)=d_s\times q\times d_s e^{\mathbf{i}kx\cdot d_s}$ be the plane incident wave, where $d_s,q\in S^2$. Denote the corresponding scattering field and far field pattern $E^s_{\mathrm{pl}}(x,d_s,q)$ and $E^\infty_{\mathrm{pl}}(\hat{x},d_s,q)$. Let $E^i_{\mathrm{ps}}(x,y,p)=\mathbb{G}(x,y)p$ be the point source excitation at $y$ in the polarization $p$ and denote the corresponding scattering field and far field pattern $E^s_{\mathrm{ps}}(x,y,p)$ and $E^\infty_{\mathrm{ps}}(\hat{x},y,p)$. The following lemma is proved in [28, Theorem 2.3.4].

Lemma 4.5. *For scattering by a perfect conductor we have*

$$E_{\rm ps}^{\infty}(\hat{x},y,p)\cdot q=\frac{1}{4\pi}E_{\rm pl}^{s}(y,-\hat{x},q)\cdot p,$$

*for any* $\hat{x}\in S^2, y\in\mathbb{R}^3\backslash\bar{D}$ *and* $p,q\in S^2$.

The following estimate for the far field pattern will be used in our analysis and will be proved in the appendix of this paper.

Lemma 4.6. *We have*

$$|E_{\rm pl}^{\infty}(\hat{x}_s,-\hat{x}_r,p)|+|\nabla_{T,\hat{x}_s}E_{\rm pl}^{\infty}(\hat{x}_s,-\hat{x}_r,p)|\le Cd_D(1+\|G_e\|),$$

*where the constant* $C$ *depends on* $kd_D$ *but is independent of* $k$. $\nabla_{T,\hat{x}_s}E_{\rm pl}^{\infty}(\hat{x}_s,-\hat{x}_r,p)$ *is the tangential derivative of* $E_{\rm pl}^{\infty}(\hat{x}_s,-\hat{x}_r,p)$ *in* $\hat{x}_s$.

Lemma 4.7. *Let* $h\in C^1(S^2)$ *and define*

$$v(\hat{x}_r)=\int_{S^2}h(\hat{x}_s)e^{-2\mathbf{i}kR_s|\tau\hat{x}_r-\hat{x}_s|}d\hat{x}_s,\qquad\forall\hat{x}_r\in S^2.$$

*There exists a constant* $C>0$ *independent of* $k,R_s,\tau$ *such that*

$$|v(\hat{x}_r)|\le C(kR_s)^{-1}(\|h\|_{L^\infty(S^2)}+\|\nabla_T h\|_{L^\infty(S^2)}),\qquad\forall\hat{x}_r\in S^2.$$

*Proof.* Let $\mathbb{Q}_r\in\mathbb{R}^{3\times3}$ be the orthogonal matrix such that $\mathbb{Q}_r\hat{x}_r=(0,0,1)^T$, we have by the coordinate transform $\hat{y}_s=\mathbb{Q}_r\hat{x}_s$ that

$$v(\hat{x}_r)=\int_0^{2\pi}\int_0^{\pi}h(\mathbb{Q}_r^T\hat{y}_s)e^{-2\mathbf{i}kR_s\sqrt{\tau^2+1-2\tau\cos\theta}}\sin\theta d\theta d\phi,$$

where $\hat{y}_s=\mathbb{Q}_r\hat{x}_s=(\sin\theta\cos\phi,\sin\theta\sin\phi,\cos\theta)^T$, $\theta\in[0,\pi],\phi\in[0,2\pi]$. Denote the phase function $f(\theta)=\sqrt{\tau^2+1-2\tau\cos\theta}$. Since $f'(\theta)=\tau\sin\theta/f(\theta)$, by integration by parts we obtain

$$\begin{aligned}v(\hat{x}_r)=&-\frac{1}{2\mathbf{i}kR_s\tau}\int_0^{2\pi}\Big[h(\mathbb{Q}_r\hat{y}_s)f(\theta)e^{-2\mathbf{i}kR_sf(\theta)}\Big]_{\theta=0}^{\theta=\pi}d\phi\\&+\frac{1}{2\mathbf{i}kR_s\tau}\int_0^{2\pi}\int_0^{\pi}e^{-2\mathbf{i}kR_sf(\theta)}\left(\frac{\partial h(\mathbb{Q}_r\hat{y}_s)}{\partial\theta}f(\theta)+h(\mathbb{Q}_r\hat{y}_s)f'(\theta)\right)d\theta d\phi.\end{aligned}$$

The lemma now follows easily since

$$\int_0^{\pi}|f'(\theta)|d\theta=\tau\int_0^{\pi}\frac{\sin\theta}{\sqrt{\tau^2+1-2\tau\cos\theta}}d\theta\le\pi\tau.$$

This completes the proof. ■

The following lemma gives the estimate for the term $\mathrm{III}_1$.

Lemma 4.8. *We have* $|\mathrm{III}_1|\le C(1+\|G_e\|)R_s^{-1}$, *where the constant* $C$ *may depend on* $kd_D, k|z|$ *but is independent of* $k,d_D$.

*Proof.* We first observe that $||x-y|-(|x|-\hat{x}\cdot y)| \le C|y|^2/|x|$ for $|x|>|y|$. This yields, for any $z\in\Omega$,

$$g(x_r,z)=\frac{e^{\mathbf{i}kR_r}}{4\pi R_r}e^{-\mathbf{i}k\hat{x}_r\cdot z}+\gamma_1(x_r,z),\quad g(z,x_s)=\frac{e^{\mathbf{i}kR_s}}{4\pi R_r}e^{-\mathbf{i}k\hat{x}_s\cdot z}+\gamma_1(z,x_s), \tag{4.6}$$

where $|\gamma_1(x_r,z)|\le C(|z|+k|z|^2)R_r^{-2}, |\gamma_1(z,x_s)|\le C(|z|+k|z|^2)R_s^{-2}$. By definition we know that $E^s(x_r,x_s)=E^s_{\rm ps}(x_r,x_s,p)$ and thus, by Lemma 3.1, we have

$$E^s(x_r,x_s)\cdot p=\frac{e^{\mathbf{i}kR_r}}{R_r}E^\infty_{\rm ps}(\hat{x}_r,x_s,p)\cdot p+\gamma_2(x_r,x_s),$$

where $|\gamma_2(x_r,x_s)|\le Cd_D^2(1+\|G_e\|)R_s^{-1}R_r^{-2}$. By using the mixed reciprocity relation in Lemma 4.5 and Lemma 3.1 again, we then obtain

$$\begin{aligned} E^s(x_r,x_s)\cdot p&=\frac{e^{\mathbf{i}kR_r}}{4\pi R_r}E^s_{\rm pl}(x_s,-\hat{x}_r,p)\cdot p+\gamma_2(x_r,x_s)\\ &=\frac{e^{\mathbf{i}k(R_r+R_s)}}{4\pi R_sR_r}E^\infty_{\rm pl}(\hat{x}_s,-\hat{x}_r,p)\cdot p+\gamma_2(x_r,x_s)+\gamma_3(x_r,x_s), \end{aligned} \tag{4.7}$$

where $|\gamma_3(x_r,x_s)|\le Cd_D^2(1+\|G_e\|)R_r^{-1}R_s^{-2}$.

Inserting (4.6)-(4.7) into (4.5) we have

$$\mathrm{III}_1=-k^2\frac{e^{2\mathbf{i}k(R_r+R_s)}}{64\pi^3}\int_{S^2\times S^2}\psi(\hat{x}_r,\hat{x}_s)e^{-2\mathbf{i}kR_s|\tau\hat{x}_r-\hat{x}_s|}d\hat{x}_sd\hat{x}_r+\gamma_4(z),$$

where $|\gamma_4(z)|\le C(1+\|G_e\|)R_s^{-1}$ and

$$\psi(\hat{x}_r,\hat{x}_s)=E^\infty_{\rm pl}(\hat{x}_s,-\hat{x}_r,p)\cdot p\,e^{-\mathbf{i}k(\hat{x}_s+\hat{x}_r)\cdot z}. \tag{4.8}$$

By Lemma 4.7 and then (4.8)

$$\begin{aligned} |\mathrm{III}_1|&\le k^2\max_{\hat{x}_r\in S^2}\left|\int_{S^2}\psi(\hat{x}_r,\hat{x}_s)e^{-2\mathbf{i}k(\hat{x}_s+\hat{x}_r)\cdot z}d\hat{x}_s\right|\\ &\le Ck^2(kR_s)^{-1}\max_{\hat{x}_r\in S^2}(\|\psi(\hat{x}_r,\cdot)\|_{L^\infty(S^2)}+\|\nabla_{T,\hat{x}_s}\psi(\hat{x}_r,\cdot)\|_{L^\infty(S^2)})\\ &\le Ck^2(kR_s)^{-1}\max_{\hat{x}_r\in S^2}(\|E^\infty_{\rm pl}(\cdot,-\hat{x}_r,p)\|_{L^\infty(S^2)}+\|\nabla_{T,\hat{x}_s}E^\infty_{\rm pl}(\cdot,-\hat{x}_r,p)\|_{L^\infty(S^2)}). \end{aligned}$$

This completes the proof by using Lemma 4.6. ■

Now we are ready for the proof of the main theorem of this section.

*Proof of Theorem 4.1.* By (4.2), (4.4)-(4.5), Lemma 4.2-Lemma 4.4, and Lemma 4.8 we are left to show that

$$|\mathrm{II}_1-I_{\rm RTM}(z)|\le C(1+\|G_e\|)R_s^{-1} \tag{4.9}$$

for some constant $C$ that may depend on $kd_D, k|z|$ but is independent of $k, R_r, R_s$.

We follow the argument in [10] to give an outline of the proof for the sake of completeness. By the integral representation formula, we have

$$E^s(x_r, x_s) \cdot p = \mathcal{G}(\mathbb{G}(\cdot, x_r)p, E^s(\cdot, x_s)).$$

Thus by Lemma 3.2,

$$k \int_{\Gamma_r} g(x_r, z)\overline{E^s(x_r, x_s)} \cdot p \, dx_r = \mathcal{G}(\operatorname{Im} \mathbb{G}(\cdot, z)p, \overline{E^s(\cdot, x_s)}) + \mathcal{G}(\overline{\mathbb{W}_r(\cdot, z)}p, \overline{E^s(\cdot, x_s)}),$$

where $\mathcal{G}(\cdot, \cdot)$ is the gap functional defined in (3.8). Since $\nu \times E^s(x, x_s) = -\nu \times \mathbb{G}(x, x_s)p$ on $\Gamma_D$, by Lemmas 3.2-3.3 we have

$$|\mathcal{G}(\overline{\mathbb{W}_r(\cdot, z)}p, \overline{E^s(\cdot, x_s)})| \le C d_D (1 + \|G_e\|)(R_r R_s)^{-1}. \tag{4.10}$$

Now by definition

$$\begin{aligned} \mathrm{II}_1 &= -k^2 \operatorname{Im} \int_{\Gamma_r \times \Gamma_s} g(z, x_s) g(x_r, z) \overline{E^s(x_r, x_s)} \cdot p dx_r dx_s \\ &= -\mathcal{G}(\operatorname{Im} \mathbb{G}(\cdot, z)p, V(z, \cdot)) \\ &\quad -k \operatorname{Im} \int_{\Gamma_s} g(z, x_s) \mathcal{G}(\overline{\mathbb{W}_r(\cdot, z)}p, \overline{E^s(\cdot, x_s)}) ds(x_s), \end{aligned} \tag{4.11}$$

where $V(z, x) = k \int_{\Gamma_s} g(z, x_s)\overline{E^s(x, x_s)} dx_s$. Taking the complex conjugate of the field $V(z, x)$ leads to

$$\overline{V(z, x)} = k \int_{\Gamma_s} \overline{g(z, x_s)} E^s(x, x_s) dx_s,$$

which implies $\overline{V(z, \cdot)}$ can be viewed as the linear superposition of the scattering field $E^s(\cdot, x_s)$. Thus

$$\operatorname{curl} \operatorname{curl} \overline{V(z, x)} - k^2 \overline{V(z, x)} = 0 \quad \text{in } \mathbb{R}^3 \backslash \bar{D},$$

and on the boundary of the obstacle $D$, we have

$$\begin{aligned} \nu \times \overline{V(z, x)} &= \nu \times k \int_{\Gamma_s} \overline{g(z, x_s)} E^s(x, x_s) dx_s \\ &= -\nu \times k \int_{\Gamma_s} \overline{g(z, x_s)} \mathbb{G}(x, x_s) p dx_s \\ &= -\nu \times \operatorname{Im} \mathbb{G}(x, z)p - \nu \times \mathbb{W}_s(x, z)p. \end{aligned}$$

This implies $V(x, z) = \overline{\Psi(x, z)} + V_1(z, x)$, where $\Psi(x, z)$ is the solution of (3.9)-(3.11) and $V_1(z, x)$ is the scattering solution of (3.3)-(3.4) with $g(x) = -\nu \times \overline{\mathbb{W}_s(x, z)}p$. Thus we obtain

$$\begin{aligned} \mathrm{II}_1 &= -\operatorname{Im} \mathcal{G}(\operatorname{Im} \mathbb{G}(\cdot, z)p, \overline{\Psi(\cdot, z)}) - \operatorname{Im} \mathcal{G}(\operatorname{Im} \mathbb{G}(\cdot, z)p, V_1(z, \cdot)) \\ &\quad -k \operatorname{Im} \int_{\Gamma_s} g(z, x_s) \mathcal{G}(\overline{\mathbb{W}_r(\cdot, z)}p, \overline{E^s(\cdot, x_s)}) ds(x_s) \end{aligned} \tag{4.12}$$

Since $\nu \times \Psi(x,z)p$ is real on $\Gamma_D$ by (3.10), we obtain by (3.7) that

$$
\begin{aligned}
-\operatorname{Im}\mathcal{G}(\operatorname{Im}\mathbb{G}(\cdot,z)p,\overline{\Psi(\cdot,z)}) &= \operatorname{Im}\int_{\Gamma_D}\left[\Psi(x,z)\cdot\nu\times\operatorname{curl}\overline{\Psi(x,z)}\right]ds \\
&= k\int_{S^2}|\Psi^\infty(\hat{x},z)|^2 d\hat{x}. \qquad (4.13)
\end{aligned}
$$

Since $\operatorname{Im}\mathbb{G}(x,z)p$ and $V_1(z,x)$ satisfy Maxwell equation outside $D$, we obtain by integration by parts that

$$
\begin{aligned}
&\mathcal{G}(\operatorname{Im}\mathbb{G}(\cdot,z)p, V_1(z,\cdot)) \\
&= \int_{\Gamma_D}\left[\operatorname{Im}\mathbb{G}(x,z)p\cdot\nu\times\operatorname{curl}V_1(z,x) - \nu\times\operatorname{curl}\left(\operatorname{Im}\mathbb{G}(x,z)p\right)\cdot V_1(z,x)\right]ds \\
&= \int_{\Gamma_s}\left[\operatorname{Im}\mathbb{G}(x_s,z)p\cdot\nu\times\operatorname{curl}V_1(z,x_s) - \nu\times\operatorname{curl}\left(\operatorname{Im}\mathbb{G}(x,z)p\right)\cdot V_1(z,x_s)\right]ds(x_s).
\end{aligned}
$$

By the integral representation formula we know that $V_1(z,x_s) = \mathcal{G}(\mathbb{G}(x_s,\cdot)q, V_1(z,\cdot))$, which implies by the fact that $V_1(z,x)$ is the scattering solution of (3.3)-(3.4) with $g(x) = -\nu\times\overline{\mathbb{W}_s(x,z)}p$ and Lemma 3.3 that

$$
|V_1(z,x_s)| \le Cd_D(1+\|G_e\|)R_s^{-2}, \quad |\operatorname{curl}V_1(z,x_s)| \le C(1+\|G_e\|)R_s^{-2}.
$$

Thus

$$
|\mathcal{G}(\operatorname{Im}\mathbb{G}(\cdot,z)p, V_1(z,\cdot))| \le C(1+\|G_e\|)R_s^{-1}. \qquad (4.14)
$$

Finally by (4.10) it is easy to see that

$$
\left|k\operatorname{Im}\int_{\Gamma_s} g(z,x_s)\mathcal{G}(\overline{\mathbb{W}_r(\cdot,z)}p, \overline{E^s(\cdot,x_s)})ds(x_s)\right| \le C(1+\|G_e\|)R_s^{-1}. \qquad (4.15)
$$

This completes the proof by (4.12)-(4.15). □

To conclude this section we remark that Theorem 4.1 can also be proved for the imaging of impedance non-penetrable and penetrable obstacles with phaseless data by modifying the argument in this section and the proof in [10, Theorem 3.1, Theorem 3.2]. We recall that for the imaging of impedance non-penetrable obstacles with the phaseless data, the measured phaseless total field $|E(x_r,x_s)\cdot p| = |E^s(x_r,x_s)\cdot p + E^i(x_r,x_s)\cdot p|$, where $E^s(x_r,x_s)$ is the radiation solution of the Maxwell problem

$$
\begin{aligned}
&\operatorname{curl}\operatorname{curl}E^s - k^2E^s = 0 \quad \text{in } \mathbb{R}^3\backslash\bar{D}, \\
&\nu\times\operatorname{curl}E^s - \mathbf{i}k\eta(x)(\nu\times E^s\times\nu) = -(\nu\times\operatorname{curl}E^i - \mathbf{i}k\eta(x)(\nu\times E^i\times\nu)) \text{ on } \Gamma_D, \\
&r\left(\operatorname{curl}E^s\times\hat{x} - \mathbf{i}kE^s\right)\to 0 \quad \text{as } r=|x|\to\infty.
\end{aligned}
$$

Here $\eta(x) > 0$ is the impedance function. For penetrable obstacles, the measured total field $|E(x_r,x_s)\cdot p| = |E^s(x_r,x_s)\cdot p + E^i(x_r,x_s)\cdot p|$, where $E^s(x_r,x_s)$ is the radiation solution of the following problem

$$
\operatorname{curl}\operatorname{curl}E^s - k^2n(x)E^s = k^2(n(x)-1)E^i \ \text{ in } \mathbb{R}^3
$$

with $n(x)\in L^\infty(\mathbb{R}^2)$ being a positive function which is equal to 1 outside the scatterer $D$. We leave the extension to the interested readers.

**Figure 2.** *Example 5.1. The first and second column are the imaging results when the polarization direction $p = e_1$ and $p = e_2$, respectively. The last column is the imaging results of the summation of the first and second column.*

**5. Numerical Examples.** In this section, we show a variety of numerical experiments to illustrate the effectiveness of the RTM algorithm with 2D and 3D phaseless electromagnetic total field data in this paper. The boundaries of the obstacles used in our 2D numerical experiments are parameterized as follows:

$$\begin{aligned}
\text{Circle:} \quad & x_1 = \rho\cos(\theta), \quad x_2 = \rho\sin(\theta), \quad \theta \in (0, 2\pi], \\
\text{Kite:} \quad & x_1 = \cos(\theta) + 0.65\cos(2\theta) - 0.65, \quad x_2 = 1.5\sin(\theta), \quad \theta \in (0, 2\pi], \\
p\text{-leaf:} \quad & r(\theta) = 1 + 0.2\cos(p\theta), \quad \theta \in (0, 2\pi], \\
\text{Rounded-square:} \quad & x_1 = \cos^3(\theta) + \cos(\theta), \quad x_2 = \sin^3(\theta) + \sin(\theta).
\end{aligned}$$

**5.1. Numerical examples in 2D.** We first show the efficiency of our imaging algorithm in the setting of transverse electric (TE) case, that is, the electromagnetic waves are independent of $x_3$ direction. In this subsection all the vector fields are assumed to be two dimensional. Let $p = (p_1, p_2)^T$ be the polarization direction and $g(x, x_s) = \frac{\mathbf{i}}{4} H_0^{(1)}(k|x - x_s|)$ be the fundamental solution of the two-dimensional Helmholtz equation with the source at $x_s \in \mathbb{R}^2$. The incident

**Figure 3.** *Example 5.2. From left to right: imaging results for non-penetrable obstacles with the impedance $\eta = 0.1$, $\eta = 1$, and a penetrable obstacle with the diffractive index $n(x) = 0.5$ by the summation of the imaging function of two polarization directions $p = e_1$ and $p = e_2$.*

electric field $E^i(x, x_s) = \mathbb{G}(x, x_s)p$, where $\mathbb{G}(x, x_s) = (\mathbb{I}_2 + \frac{\nabla\nabla}{k^2})g(x, x_s)$ is the two-dimensional dyadic Green function. To synthesize the scattering data we use the magnetic field integral equation (MFIE) method proposed in [26] to obtain the equivalent surface currents then produce the scattering electric field at the receivers. The MFIE integral equations on $\Gamma_D$ are solved on the uniform mesh of the boundary with ten points per probe wavelength.

Example 5.1. *We consider the imaging of single perfect conducting obstacles of three kinds of shape: circle, rounded-square and 3-leaf. The incident wavenumber is $k = 4\pi$. The sources and receivers are evenly distributed at the circle of radius $R_s = 10$ and $R_r = 11$, respectively. The number of sources and receiver is equal: $N_s = N_r = 256$. The search domain is $\Omega = [-4, 4] \times [-4, 4]$ with the sampling grid $201 \times 201$.*

Figure 2 shows the imaging results for these three kinds of shape with single polarization direction or two polarization directions. We can see that the obstacles can be well recovered by our phaseless imaging function even with only one polarization direction.

Example 5.2. *We consider the imaging of non-penetrable obstacles with impedance function $\eta = 0.1$ and $\eta = 1$, and a penetrable obstacle with diffractive index $n(x) = 0.5$ by summing the imaging results of two polarization directions. The parameters used in this example is the same as those in Example 5.1.*

Figure 3 shows the imaging results for non-penetrable with impedance boundary condition and penetrable obstacle, which indicates clearly the effectiveness of our imaging algorithm for different type of obstacles.

Example 5.3. *We consider the stability of the imaging function with respect to additive Gaussian random noises. We introduce the additive Gaussian noise as follows (see e.g. [9]):*

$$|E(x_r, x_s)\cdot p|_{\text{noise}} = |E(x_r, x_s)\cdot p + \nu_{\text{noise}}|,$$

*where $E(x_r, x_s)\cdot p$ is the phaseless synthesized total field data and $\nu_{\text{noise}}$ is the Gaussian noise with mean zero and standard deviation $\mu$ times the maximum of the data $|E(x_r, x_s)\cdot p|$, i.e. $\nu_{\text{noise}} = \mu \max |E(x_r, x_s)\cdot p|\varepsilon$, and $\varepsilon \sim \mathcal{N}(0, 1)$.*

Figure 4 and Figure 5 show the imaging results using single frequency data added with Gaussian noise level $\mu = 2\%, 4\%, 8\%, 10\%$ for incident wavenumber $k = 4\pi$ and $k = 6\pi$,

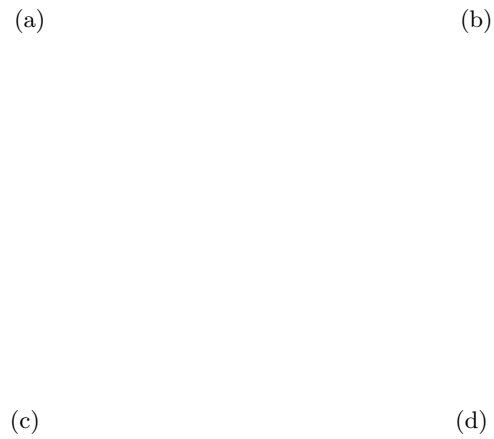


**Figure 4.** *Example 5.3: The imaging results using single frequency data with additive Gaussian noise* $\mu = 2\%, 4\%, 8\%, 10\%$ *from* $(a)$ *to* $(d)$*, respectively. The probe wavelength is* $\lambda = 0.5$*.*

respectively. The imaging quality can be improved by using multi-frequency data as illustrated in Figure 6 in which we show the imaging results added with the noise level $\mu = 2\%, 4\%, 8\%, 10\%$ Gaussian noise by summing the imaging functions for six probed wavenumbers $k = 4\pi, 4.4\pi, 4.8\pi, 5.2\pi, 5.6\pi, 6.0\pi$.

**5.2. Numerical examples in 3D.** In this subsection, we apply our direct imaging method to phaseless electromagnetic imaging problem in 3D. Here we consider the imaging of perfect conducting objects. To obtain the synthetic data, we use the finite element package PHG [27] to solve the 3D forward problem. The method of the perfectly matched layer (PML) is used to truncate the computational domain [8]. The finite element mesh is generated by using NETGEN [24]. The PML equation is discretized by using the lowest order Nedelec edge element and the resulting linear system of equations is solved by the GMRES [29] method preconditioned by an algebraic multigrid (AMG) solver [30].

Example 5.4. *We consider imaging a perfectly conducting sphere and a calabash-like obstacle. The imaging domain is* $\Omega = (-2, 2)\times(-2, 2)\times(-2, 2)$ *with the sampling mesh* $80\times80\times80$*. The incident wavenumber is* $k = 2\pi$*,* $N_s = N_r = 256$*, and* $R_r = R_s = 10$*.*

The imaging results are showed in Figures 7, 8 and 9. We observe that the imaging function proposed in this paper can reconstruct the shape of the obstacles quite well without

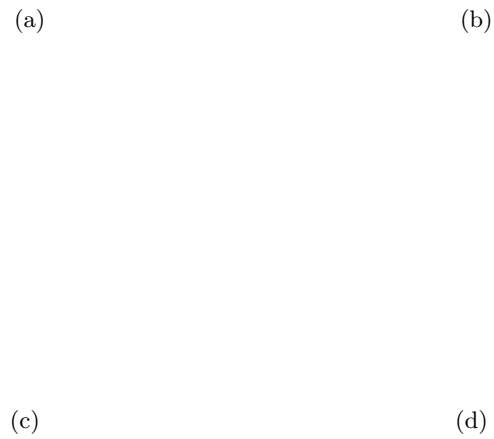


**Figure 5.** *Example 5.3: The imaging results using single frequency data with additive Gaussian noise* $\mu = 2\%, 4\%, 8\%, 10\%$ *from* $(a)$ *to* $(d)$*, respectively. The probe wavelength is* $\lambda = 1/3$.

the phase information.

**6. Appendix.** In the section we study the high frequency limit of the RTM imaging function and give the proofs of Lemma 3.1 and Lemma 4.6.

**6.1. The RTM imaging function in high frequency limit.** In this subsection we consider the high frequency limit $k \gg 1$ of the RTM imaging function $I_{\rm RTM}(z)$ in (1.4) when $z \in \Gamma_D$. For simplicity we assume the obstacle is smooth and strictly convex. For any $\xi \in \mathbb{R}^3 \backslash \bar{D}$ far away from the scatterer and $q \in S^2$, let $\mathbb{G}_D(x, \xi)q$ be be the Green function which satisfies

$$\begin{aligned}
&\operatorname{curl}\operatorname{curl}\left(\mathbb{G}_D(x,\xi)q\right) - k^2\mathbb{G}_D(x,\xi) = \delta_\xi(x)q \quad \text{in } \mathbb{R}^3\backslash\bar{D},\\
&\nu \times \mathbb{G}_D(x,\xi)q = 0 \quad \text{on } \Gamma_D,\\
&r\left(\operatorname{curl}\left(\mathbb{G}_D(x,\xi)q\right) \times \hat{x} - \mathbf{i}k\mathbb{G}_D(x,\xi)q\right) \to 0 \quad \text{as } r = |x| \to \infty.
\end{aligned}$$

The solution to the problem (3.9)-(3.11) can be expressed by using the integral representation theorem that

$$\Psi(z,\xi)\cdot q = \int_{\partial D} \nu \times \left(\operatorname{curl}\mathbb{G}_D(x,\xi)q\right)\cdot\Psi(x,z)ds. \tag{6.1}$$

(a) (b)

(c) (d)

**Figure 6.** *Example 5.3: The imaging results using multi-frequency data with additive Gaussian noise* $\mu = 2\%, 4\%, 8\%, 10\%$ *from* $(a)$ *to* $(d)$*, respectively. The probe wavelengths are* $\lambda = 1/2, 1/2.2, 1/2.4, 1/2.6, 1/2.8, 1/3$.

For $x \in \Gamma_D$, from the proof of Lemma 3.1 we know that

$$\mathbb{G}(x,\xi)q = \frac{e^{\mathbf{i}k|\xi|}}{4\pi|\xi|}(\hat{\xi}\times q\times\hat{\xi})e^{-\mathbf{i}k\hat{\xi}\cdot x} + O(k^{-1}|\xi|^{-2}),$$

which implies for $\xi$ far away from the scatterer, $\mathbb{G}(x,\xi)q$ can be approximated by the plane wave $\frac{e^{\mathbf{i}k|\xi|}}{4\pi|\xi|}(\hat{\xi}\times q\times\hat{\xi})e^{-\mathbf{i}k\hat{\xi}\cdot x}$. Thus by the high frequency physical optics approximation [20, Chapter 10, section 13], we have, for $\xi$ far away from the scatterer,

$$\operatorname{curl}\mathbb{G}_D(x,\xi)q \approx \begin{cases} 2\operatorname{curl}\left[\frac{e^{\mathbf{i}k|\xi|}}{4\pi|\xi|}(\hat{\xi}\times q\times\hat{\xi})e^{-\mathbf{i}k\hat{\xi}\cdot x}\right] & \text{if } x\in\partial D^+_{\hat{\xi}},\\ 0 & \text{if } x\in\partial D^-_{\hat{\xi}},\end{cases}$$

where $\partial D^+_{\hat{\xi}} = \{x\in\Gamma_D : \nu(x)\cdot\hat{\xi} > 0\}$ and $\partial D^-_{\hat{\xi}} = \{x\in\Gamma_D : \nu(x)\cdot\hat{\xi} < 0\}$ are respectively the illuminated and shadow region of the incident plane wave $\frac{e^{\mathbf{i}k|\xi|}}{4\pi|\xi|}(\hat{\xi}\times q\times\hat{\xi})e^{-\mathbf{i}k\hat{\xi}\cdot x}$. Thus, by simple calculation,

$$\operatorname{curl}\mathbb{G}_D(x,\xi)q \approx \begin{cases} 2\mathbf{i}k\,\frac{e^{\mathbf{i}k|\xi|}}{4\pi|\xi|}q\times\hat{\xi} & \text{if } x\in\partial D^+_{\hat{\xi}},\\ 0 & \text{if } x\in\partial D^-_{\hat{\xi}},\end{cases}$$

**Figure 7.** *The imaging of a perfect conducting sphere. From top to bottom: the imaging results for the polarization direction $p = e_1, e_2, e_3$, respectively. From left to right: the imaging results of the cross-section $x_1 = 0, x_2 = 0, x_3 = 0$, respectively.*

which implies from (6.1) that

$$\Psi(z,\xi)\cdot q \approx \frac{\mathbf{i}k}{2\pi}\frac{e^{\mathbf{i}k|\xi|}}{|\xi|}\int_{\partial D_\xi^+}(\nu\times q\times\hat{\xi})\cdot\Psi(x,z)e^{-\mathbf{i}k\hat{\xi}\cdot x}ds.$$

Let $t=(t_1,t_2)\in T_{\hat{\xi}}\subset\mathbb{R}^2$ be the parametrization of the boundary $\partial D_{\hat{\xi}}^+$, then

$$\Psi(z,\xi)\cdot q \approx \frac{\mathbf{i}k}{2\pi}\frac{e^{\mathbf{i}k|\xi|}}{|\xi|}\int_{T_{\hat{\xi}}}(\hat{\xi}\times q)\cdot(\nu\times\Psi(x(t),z))e^{-\mathbf{i}k\hat{\xi}\cdot x(t)}\left|\frac{\partial x}{\partial t_1}\times\frac{\partial x}{\partial t_2}\right|dt.$$

Now we are going to use the principle of the stationary phase to above oscillatory integral. Let $\phi(t_1,t_2)=-\hat{\xi}\cdot x(t_1,t_2)$ be the phase function. Since $D$ is strictly convex, there is only one point $x(\hat{\xi})=x(t(\hat{\xi}))\in\partial D_{\hat{\xi}}^+$ such that $\nabla\phi(t(\hat{\xi}))=0$ which satisfies $\nu(x(\hat{\xi}))=\hat{\xi}$. The determinant of the Hessian matrix of the phase function at $x(\hat{\xi})$ is

$$\det\nabla^2\phi(t(\hat{\xi}))=\Big(\hat{\xi}\cdot\frac{\partial^2 x}{\partial t_1^2}\Big)\Big(\hat{\xi}\cdot\frac{\partial^2 x}{\partial t_2^2}\Big)-\Big(\hat{\xi}\cdot\frac{\partial^2 x}{\partial t_1\partial t_2}\Big)^2=\kappa(x(\hat{\xi}))\left|\frac{\partial x}{\partial t_1}(t(\hat{\xi}))\times\frac{\partial x}{\partial t_2}(t(\hat{\xi}))\right|^2,$$

**Figure 8.** *The imaging of a perfect conducting Calabash-like obstacle. From top to bottom: the imaging results for the polarization direction $p = e_1, e_2, e_3$, respectively. From left to right: the imaging results of the cross-section $x_1 = 0, x_2 = 0, x_3 = 0$, respectively.*

where $\kappa(x)$ is the Gaussian curvature and we have used the fact that $\hat{\xi} = \nu(x(\hat{\xi}))$. By the theorem of stationary phase [17, Theorem 7.7.5], we obtain

$$\begin{aligned}\Psi(z,\hat{\xi})\cdot q &\approx \frac{\mathbf{i}k}{2\pi}\frac{e^{\mathbf{i}k|\xi|}}{|\xi|}(\hat{\xi}\times q)\cdot(\nu(x(\hat{\xi}))\times\Psi(x(\hat{\xi}),z))e^{-\mathbf{i}k\hat{\xi}\cdot x(\hat{\xi})}\left(\frac{k}{2\pi\mathbf{i}}\right)^{-1}\kappa(x(\hat{\xi}))^{-1/2}\\ &= \frac{e^{\mathbf{i}k|\xi|}}{|\xi|}q\cdot(\hat{\xi}\times\operatorname{Im}\mathbb{G}(x(\hat{\xi}),z)p\times\hat{\xi})e^{-\mathbf{i}k\hat{\xi}\cdot x(\hat{\xi})}\kappa(x(\hat{\xi}))^{-1/2},\end{aligned}$$

where we have used (3.10) and $\hat{\xi} = \nu(x(\hat{\xi}))$ in the last equality. Hence, by (3.6) and Theorem 3.1 we have

$$I_{\mathrm{RTM}}(z) \approx k\int_{S^2}\frac{|\hat{\xi}\times\operatorname{Im}\mathbb{G}(x(\hat{\xi}),z)p\times\hat{\xi}|^2}{\kappa(x(\hat{\xi}))}d\hat{\xi}. \tag{6.2}$$

Since $\operatorname{Im}\mathbb{G}(x(\hat{\xi}),z)p = (\mathbb{I}+\frac{\nabla_x\nabla_x}{k^2})\frac{\sin(k|x(\hat{\xi})-z|)}{4\pi|x(\hat{\xi})-z|}$, the main contribution in above integral is for $\hat{\xi}\in S^2$ such that $|x(\hat{\xi})-z|\le\lambda/2$, where $\lambda = 2\pi/k$ is the wavelength. This implies $I_{\mathrm{RTM}}(z)$ is inversely proportional to the curvature of the surface $\Gamma_D$ around $z\in\Gamma_D$.

**Figure 9.** *3D view of the imaging results by summing the imaging functions with $p = e_1, e_2, e_3$. Left column shows the true obstacles and the right column shows the imaging results.*

**6.2. Proof of Lemma 3.1.** We give a sketch of the proof to confirm the bound for $\gamma(x)$. It is easy to check that for any $q \in S^2$,

$$\mathbb{G}(x,y)q = \frac{e^{\mathbf{i}k|x|}}{4\pi|x|}e^{-\mathbf{i}k\hat{x}\cdot y}(1-\hat{x}\hat{x}^T)q + R_1(x,y), \qquad \forall x \in \mathbb{R}^3\backslash\bar{D},\ |x| \gg 1, y \in \Gamma_D,$$
$$\operatorname{curl}(\mathbb{G}(x,y)q) = \frac{\mathbf{i}ke^{\mathbf{i}k|x|}}{4\pi|x|}e^{-\mathbf{i}k\hat{x}\cdot y}\hat{x}\times q + R_2(x,y), \qquad \forall x \in \mathbb{R}^3\backslash\bar{D},\ |x| \gg 1, y \in \Gamma_D,$$

where $|R_1(x,y)| + k^{-1}|\nabla_y R_1(x,y)| \le Ck^{-1}|x|^{-2}$, $|R_2(x,y)| + k^{-1}|\nabla_y R_2(x,y)| \le C|x|^{-2}$ for some constant $C$ depending on $kd_D$ but independent of $k, d_D$. Inserting these two asymptotic formulae to the integral representation for the scattering solution $U$ one obtains

$$\gamma(x) = \int_{\Gamma_D} \left(R_1(x,y)\cdot\nu \times \operatorname{curl} U(y) - \nu \times R_2(x,y)\cdot U(y)\right) ds(y). \tag{6.3}$$

Now by using (3.1) and the definition of the norm of $H^{-1/2}(\mathrm{div};\Gamma_D)$ we have

$$\begin{aligned}&\left|\int_{\Gamma_D} R_1(x,y)\cdot\nu\times\operatorname{curl}U(y)ds(y)\right|\\ &\le Cd_D\|R_1(x,\cdot)\|_{H^{1/2}(\Gamma_D)}\cdot k\|G_e\|\|\nu\times U\|_{H^{-1/2}(\mathrm{div};\Gamma_D)}\\ &\le Cd_D^{3/2}\|G_e\||x|^{-2}\|\|g\|_{H^{-1/2}(\mathrm{div};\Gamma_D)}.\end{aligned}$$

Similarly

$$\left|\int_{\Gamma_D}\nu\times R_2(x,y)\cdot U(y)ds(y)\right|\le Cd_D^{3/2}|x|^{-2}\|\|g\|_{H^{-1/2}(\mathrm{div};\Gamma_D)}.$$

This completes the proof. □

**6.3. Proof of Lemma 4.6.** By the definition the far field pattern in (3.5) we have

$$\begin{aligned}&E_{\mathrm{pl}}^{\infty}(\hat{x}_s,-\hat{x}_r,p)\\ &=\frac{1}{4\pi}\hat{x}_s\times\int_{\Gamma_D}\left[\nu\times\operatorname{curl}E_{\mathrm{pl}}^{s}(x,-\hat{x}_r,p)\times\hat{x}_s+\mathbf{i}k\nu\times E_{\mathrm{pl}}^{s}(x,-\hat{x}_r,p)\right]e^{-\mathbf{i}k\hat{x}_s\cdot x}ds(x).\end{aligned}$$

Since $\nu\times E_{\mathrm{pl}}^{s}(x,-\hat{x}_r,p)=-\nu\times[(\hat{x}_r\times p\times\hat{x}_r)e^{-\mathbf{i}k\hat{x}_r\cdot x}]$ on $\Gamma_D$, by (3.2), there exists a constant $C$ independent of $k,d_D$ such that

$$\begin{aligned}\|\,\nu\times\operatorname{curl}E_{\mathrm{pl}}^{s}(x,-\hat{x}_r,p)\,\|_{H^{-1/2}(\mathrm{div};\Gamma_D)}&\le k\|G_e\|\|\,\nu\times E_{\mathrm{pl}}^{s}(x,-\hat{x}_r,p)\,\|_{H^{-1/2}(\mathrm{div};\Gamma_D)}\\ &\le k\|G_e\|\cdot Cd_D^{1/2}(1+kd_D).\end{aligned}$$

Thus for any $q\in S^2$,

$$\begin{aligned}&|E_{\mathrm{pl}}^{\infty}(\hat{x}_s,-\hat{x}_r,p)\cdot q|\\ &\le d_D\|\,\nu\times\operatorname{curl}E_{\mathrm{pl}}^{s}(\cdot,-\hat{x}_r,p)\,\|_{H^{-1/2}(\mathrm{div};\Gamma_D)}\|\hat{x}_s\times\hat{x}_s\times qe^{-\mathbf{i}k\hat{x}_r\cdot x}\|_{H^{1/2}(\Gamma_D)}\\ &\quad+k|\Gamma_D|\|\nu\times E_{\mathrm{pl}}^{s}(\cdot,-\hat{x}_r,p)\|_{L^{\infty}(\Gamma_D)}\\ &\le Ck\|G_e\|d_D^2(1+kd_D)^2+Ckd_D^2,\end{aligned}$$

where the constant $C$ is independent of $k,d_D$. This proves the first estimate of the lemma. The second estimate in the lemma can be proved similarly. □

**Acknowledgement.** The authors would like to thank the referees for the helpful comments that greatly improved the paper.

## REFERENCES

[1] P. Bardsley and F. Vasquez, *Kirchhoff migration without phases*, arXiv: 1601.02667.
[2] G. Bao, P. Li, and J. Lv, *Numerical solution of an inverse diffraction grating problem from phaseless data,* J. Opt. Soc. Am. A, 30 (2013), pp. 293-299.
[3] N. Bleistein, J. Cohen, and J. Stockwell, *Mathematics of Multidimensional Seismic Imaging, Migration, and Inversion*, Springer, New York, 2001.

[4] A. Buffa, M. Costabel, and D. Sheen, *On traces for $H(\mathrm{curl};\Omega)$ in Lipschitz domains,* J. Math. Anal. Appl., 276 (2002), pp. 845-867.
[5] R. Burridge and G. Beylkin, *On double integrals over spheres*, Inverse Problems, 4 (1988), pp. 1-10.
[6] E. Candes, T. Strohmer, and V. Voroninski, *Phaselift: Exact and stable signal recovery from magnitude measurements via convex programming*, Communications on Pure and Applied Mathematics 66 (2013), pp. 1241-1274.
[7] A. Chai, M. Moscoso, and G. Papanicolaou, *Array imaging using intensity-only measurements*, Inverse Problems, (27) 2010, 015005 (20pp).
[8] J. Chen and Z. Chen, *An adaptive perfectly matched layer technique for 3-D time-harmonic electromagnetic scattering problems*, Math. Comp., 77 (2008), pp. 673-698.
[9] J. Chen, Z. Chen, and G. Huang, *Reverse time migration for extended obstacles: acoustic waves*, Inverse Problems, 29 (2013), 085005 (17pp).
[10] J. Chen, Z. Chen, and G. Huang, *Reverse time migration for extended obstacles: electromagnetic waves*, Inverse Problems, 29 (2013), 085006 (17pp).
[11] Z. Chen and G. Huang, *Reverse time migration for extended obstacles: elastic waves*, (in Chinese) Sci. Sin. Math. 45 (2015), pp. 1103-1114.
[12] Z. Chen and G. Huang, *Phaseless imaging by reverse time migration: acoustic waves*, arXiv: 1502.00957.
[13] D. Colton and R. Kress, Inverse Acoustic and Electromagnetic Scattering Theory, 2nd ed., vol. 93 of Applied Mathematical Sciences, Springer-Verlag, Berlin, 1998.
[14] M. Ďurso, K. Belkebir, L. Crocco, and et al., *Phaseless imaging with experimental data: facts and challenges*, J. Opt. Soc. Am. A, 25 (2008), pp. 271-281.
[15] G. Franceschini, M.Donelli, R. Azaro, and et al., *Inversion of phaseless total field data using a two-step strategy based on the iterative multiscaling approach*, IEEE Trans. Geosci. Remote Sens., 44 (2006), pp. 3527-3539.
[16] R. Gerchberg and W.O. Saxton, *A practical algorithm for the determination of phase from image and diffraction plane pictures*, Optik 35 (1972), pp. 237-246.
[17] L. Hörmander, The Analysis of Linear Partial Differential Operators I, Springer-Verlag, Berlin, 1990.
[18] G. Leone and R, Pierri, *Reflector antenna diagnosis from phaseless data*, IEEE Trans. on Antennas and Propagation, 45 (1997), pp. 1236-1244.
[19] A. Litman and K. Belkebir, *Two-dimensional inverse profiling problem using phaseless data*, J. Opt. Soc. Am. A, 23 (2006), pp. 2737-2746.
[20] A. Ishimaru, Electromagnetic Wave Propagation, Radiation, and Scattering, Prentice Hall, Englewood Cliffs, New Jersey 07632, 1991.
[21] O. Ivanyshyn and R. Kress, *Identification of sound-soft 3D obstacles from phaseless data,* Inverse Problem and Imaing, 4 (2010), pp. 131-149.
[22] O. Ivanyshyn and R. Kress, *Inverse scattering for surface impedance from phase-less far field data,* Journal of Computational Physics, 230 (2011), pp. 3443-3452.
[23] P. Monk, Finite Element Methods for Maxwell's Equations, Oxford University Press, Oxford, 2003.
[24] NETGEN, Automatic 3D tetrahedral mesh generator, available online at http://www.hpfem.jku.at/netgen/.
[25] A. Novikov, M. Moscoso, and G. Papanicolaou, *Illumination strategies for intensity-only imaging*, SIAM J. Imag. Sci. 8 (2015), pp. 1547-1573.
[26] A. Peterson, S. Ray, and R. Mittra, Computational Methods for Electromagnetics, IEEE Press, New York, 1998
[27] PHG, Parallel Hierarchical Grid, available online at http://lsec.cc.ac.cn/phg/.
[28] R. Potthast, Point-sources and Multipoles in Inverse Scattering Theory, Chapman and Hall/CRC, Boca Raton, Florida, 2001.
[29] Y. Saad and M. Schultz, *GMRES: A generalized minimal residual algorithm for solving nonsymmetric linear systems*, SIAM J. Sci. and Stat. Comput., 7 (1986), pp. 856-869.
[30] U. Yang, *BoomerAMG: a parallel algebraic multigrid solver and preconditioner*, Appl. Numer. Math., 41 (2002) : pp. 155-177.
[31] W. Zhang, L. Li, and F. Li, *Inverse scattering from phaseless data in the freespace*, Science in China Series F: Information Sciences, 52 (2009), pp. 1389-1398.